Cancer Research

PGC1α Suppresses Prostate Cancer Cell Invasion through ERRα Transcriptional Control

Lorea Valcarcel-Jimenez[1], Alice Macchia[1], Eva Crosas-Molist[2,3], Ariane Schaub-Clerigué[1], Laura Camacho[1,4], Natalia Martín-Martín[1,5], Paolo Cicogna[1], Cristina Viera-Bardón[1,5], Sonia Fernández-Ruiz[1,5], Irene Rodriguez-Hernandez[2,3], Ivana Hermanova[1], Ianire Astobiza[1,5], Ana R. Cortazar[1,5], Jon Corres-Mendizabal[1], Antonio Gomez-Muñoz[4], Victoria Sanz-Moreno[2,3], Verónica Torrano[1,4,5], and Arkaitz Carracedo[1,4,5,6]

Abstract

The PPARγ coactivator 1 alpha (PGC1α) is a prostate tumor suppressor that controls the balance between anabolism and catabolism. PGC1A downregulation in prostate cancer is causally associated with the development of metastasis. Here we show that the transcriptional complex formed by PGC1α and estrogen-related receptor 1 alpha (ERRα) controls the aggressive properties of prostate cancer cells. PGC1α expression significantly decreased migration and invasion of various prostate cancer cell lines. This phenotype was consistent with remarkable cytoskeletal remodeling and inhibition of integrin alpha 1 and beta 4 expression, both *in vitro* and *in vivo*. CRISPR/Cas9-based deletion of ERRα suppressed PGC1α regulation of cytoskeletal organization and invasiveness. Mechanistically, PGC1α expression decreased MYC levels and activity prior to inhibition of invasiveness. In addition, PGC1α and ERRα associated at the MYC promoter, supporting the inhibitory activity PGC1α. The inverse correlation between PGC1α–ERRα activity and MYC levels was corroborated in multiple prostate cancer datasets. Altogether, these results support that PGC1α–ERRα functions as a tumor-suppressive transcriptional complex through the regulation of metabolic and signaling events.

Significance: These findings describe how downregulation of the prostate tumor suppressor PGC1 drives invasiveness and migration of prostate cancer cells.

Introduction

The process of cellular transformation stems from the acquisition of genomic aberrations that altogether change the response of normal cells and enable them with hallmarks of cancer (1, 2). The mutational landscape changes within and among tumors and along time following evolutionary principles (3). In addition, nongenomic alterations harness great relevance in the process of cancer progression. Indeed, transcriptional regulation in cancer is an emerging aspect that provides a feasible explanation to the rapid adaptation of transformed cells to hostile environments (4). Yet, the control of oncogenic and tumor-suppressive transcriptional programs remains poorly characterized.

Transcriptional coregulators encompass a family of versatile modulators of gene expression (5). These proteins harbor the capacity of controlling distinct transcriptional programs based on their partner transcription factors. In turn, transcriptional coregulators operate in a tissue- and context-specific manner, thus revealing them as major players in cell and organismal homeostasis. Among this family of genes, the PPARγ coactivator 1 alpha (PGC1α) controls biological responses in health and disease (6, 7). PGC1α is a tightly regulated protein that interacts with a variety of transcription factors, including estrogen-related receptor 1 alpha (ERRα), PPARs, and nuclear factor erythroid 2-like 2 (NFE2L2, NRF2; ref. 6). As a consequence, PGC1α coordinates metabolic and antioxidant responses, which account for its relevance in diabetes, neurodegeneration, cardiomyopathy, and cancer (7, 8).

The role of PGC1α in cancer is largely tumor type and context-dependent. On the one hand, this transcriptional coregulator favors survival, proliferation, stem cell maintenance, and therapy resistance in pancreatic tumors, breast cancer, and melanoma cells (9–14). On the other hand, we and others have demonstrated that PGC1α expression is reduced in renal and prostate carcinoma, as well as in metastatic melanoma, where it opposes the acquisition of aggressive features (15–17). The predominant mechanism of action of PGC1α in cancer biology is ascribed to

[1]CIC bioGUNE, Bizkaia, Spain. [2]Barts Cancer Institute, Queen Mary University of London, London, United Kingdom. [3]Randall Centre for Cell & Molecular Biophysics, King's College London, London, United Kingdom. [4]Biochemistry and Molecular Biology Department, University of the Basque Country (UPV/EHU), Bilbao, Spain. [5]CIBERONC, Madrid, Spain. [6]Ikerbasque, Basque Foundation for Science, Bilbao, Spain.

Note: Supplementary data for this article are available at Cancer Research Online (http://cancerres.aacrjournals.org/).

L. Valcarcel-Jimenez and A. Macchia contributed equally to this article as first authors.

V. Torrano and A. Carracedo contributed equally to this article as last authors.

Corresponding Authors: Arkaitz Carracedo, CICbioGUNE, PARQUE TECNOLOGICO DE BIZKAIA, Derio, Bizkaia 48160, Spain. Phone: 34-94406130; Fax: 34-94406130; E-mail: acarracedo@cicbiogune.es; and Verónica Torrano, Biochemistry and Molecular Biology Department, University of the Basque Country (UPV/EHU), Barrio Sarriena s/n, Leioa, Bizkaia 48940, Spain. Phone: 34-946015925; E-mail: vtorrano@cicbiogune.es

Cancer Res 2019;79:6153–65

doi: 10.1158/0008-5472.CAN-19-1231

the regulation of metabolism. This coregulator promotes the expression of genes that mediate mitochondrial biogenesis, oxidative metabolism, and the production of glutathione. In turn, PGC1α enhances the oxidative utilization of nutrients and antioxidant production. However, emerging data suggest that a fraction of the activities of PGC1α relies neither on the regulation of metabolism nor on its main partner, ERRα (16).

In prostate cancer, PGC1α suppresses cell proliferation, anchorage-independent growth, tumor burden, and metastasis (17). This coregulator is profoundly downregulated in localized prostate cancer, with a further decrease in metastatic specimens (17). Moreover, reduced PGC1α expression is associated to shorter time to biochemical recurrence after surgery, pointing at the relevance of this gene in the control of prostate cancer aggressiveness. Mechanistically, we previously showed that PGC1α requires the presence of ERRα to suppress prostate cancer cell proliferation and metastatic outgrowth, which was consistent with the reduction of biosynthetic capacity of PGC1α reexpressing cells and the elevation of nutrient catabolism (17). Moreover, a recent study revealed that the metabolic control of polyamine synthesis underlies the regulation of prostate cancer aggressiveness by this coactivator (18).

The metastatic process requires the acquisition of discreet capacities beyond cell proliferation. Specifically, the motility and invasive capacity of cancer cells are paramount for the achievement of metastasis (19). Stemming from this notion, in this study, we evaluated the contribution of PGC1α to the acquisition of these features in prostate cancer cells. Our analysis uncovers an ERRα-dependent activity of the coactivator that suppresses the acquisition of invasive properties required for prostate cancer aggressiveness.

Materials and Methods

Reagents

Doxycycline hyclate (Sigma #D9891) was used to induce gene expression or silencing in vectors under tetracycline control. Puromycin (Sigma #P8833) and blasticidin (Invitrogen #R210-01) were used for cell selection after lentiviral transfection.

Cell culture

Human prostate carcinoma cell lines PC3 and DU145 were purchased from Leibniz-Institut DSMZ-Deutsche Sammlung von Mikroorganismen und Zellkulturen GmbH, who provided authentication certificate. Cell lines where periodically subjected to microsatellite-based identity validation. None of the cell lines used in this study were found in the database of commonly misidentified cell lines maintained by the International Cell Line Authentication Committee and NCBI Biosample. 293FT cells were used for lentiviral production. All cell lines were routinely monitored for *Mycoplasma* contamination. DU145, PC3, and 293FT cell lines were maintained in DMEM supplemented with 10% volume for volume (v/v) FBS and 1% (v/v) penicillin–streptomycin. For *PGC1A* expression, cells were transduced with a modified TRIPZ (Dharmacon) doxycycline-inducible lentiviral construct in which the red fluorescent protein and miR30 region was substituted by *HA-Flag-Pgc1a* (9). For *ESRRA* deletion, single-guide RNA (sgRNA) constructs targeting *ESRRA* (sgERRα#1: 5′CTCCGGCTACCACTATGGTGTGG3′; sgERRα#2: 3′AGGAACCCTTTGGACTGTCAGGG5′) were designed using Crispor software (crispor.tefor.net) and cloned in a lentiviral vector purchased from Addgene LentiCRISPR V2 (a gift from Mohan Babu, Addgene plasmid # 83480). Lentiviral vector expressing a validated shRNA against human *MYC* from the Mission shRNA Library (TRCN0000039642) was subcloned in a Plko Tet-On inducible system (Addgene plasmid # 21915; ref. 20). Cells were transfected with lentiviral vectors following standard procedures, and viral supernatant was used to infect cells. Selection was done using puromycin (2 μg/mL) or blasticidin (for LentiCRISPR V2, 10 μg/mL) for 3 or 5 days, respectively.

Animals

All mouse experiments were carried out following the ethical guidelines established by the Biosafety and Welfare Committee at CIC bioGUNE. The procedures employed were carried out following the recommendations from Association for Assessment and Accreditation of Laboratory Animal Care International. Xenograft experiments were performed as described previously (17), injecting 1×10^6cells per tumor in two flanks of Hsd:Athymic-Nude-Foxn1nu "Nude" mouse (Envigo). Once tumors reached an average of 100 mm^3, animals were assigned to chow or doxycycline diet regime (Research diets, D12100402) and tumor volume was monitored with external caliper. After euthanasia, tumors were weighed, tissue was fresh frozen or paraffin embedded, and histologic evaluation of hematoxylin and eosin–stained sections was performed. Proliferation was assessed in paraffin-embedded tissue samples by using Ki67 antibody (MA5-14520, Thermo Fisher Scientific).

Cellular and molecular assays

Cell number quantification with crystal violet was performed as described in ref. 21.

Cell morphology and stress fiber content were examined by staining the cells with fluorescent phalloidin (Thermo Fisher Scientific F432; 1:400 dilution), a high-affinity F-actin probe. Images were taken with AxioImager D1 microscope at 200× for cell area analysis (FiJi Software) or at 400× for stress fiber quantification. Immunofluorescence detection and quantification of p-MLC (Ser19) were performed as described in ref. 22. Briefly, cells were fixed with 4% formaldehyde, permeabilized with 0.3% Triton, and incubated with primary antibody (p-MLC Ser19, Cell Signaling Technology #3672) overnight. Cells were then stained with secondary Alexa Fluor-488 or 647 anti-rabbit (Life Technologies), Alexa Fluor 546-phalloidin for F-actin detection (Life Technologies), and DAPI (Thermo Fisher Scientific D1306; 1:10,000 dilution).

For adhesion assays, cells were plated (40,000 cells/well) on a 12-well plate previously coated with rat tail collagen I (Corning 354236) at 50 μg/mL (diluted in 0.02 N of acetic acid) during 1 hour. After 30 minutes, plates were washed twice with PBS, fixed with 10% formalin, and stained with crystal violet as described previously (17).

Transwell invasion assay was carried out using Matrigel-coated chambers (BD CioCoat #354480). Cells (50,000 cells/well) were resuspended in 0.1% FBS DMEM and seeded in the top part of the chamber. In the bottom part of the well, 1.4-mL solution of complete DMEM was added. Plates were maintained at 37°C and 5% CO_2 for 48 hours. Invasion was stopped washing the well twice with PBS and using a cotton bud to remove the remaining cell of the top part of the membrane, being careful not to compromise the Matrigel. The membrane was fixed with 10% formalin (15 minutes at 4°C) and stained with crystal violet

(Sigma C3886; 0.1% crystal violet in 20% methanol). Cells were counted under the microscope. For transwell migration, chambers with membranes of 8-μm pores (BD Falcon 351185) were used. Cell plating as well as washing and fixation conditions were the same as in the invasion assay, but cells were fixed after 24 hours.

Spheroid cell culture and three-dimensional invasion assays were performed as described previously (23). Briefly, cells (700 cells/drop) were maintained in drops (25 μL/drop) with DMEM and 6% methylcellulose (Sigma M0387) on the cover of a 100-mm culture plate. Drops were incubated at 37°C and 5% CO_2 for 48 hours. Once formed, spheroids were collected, resuspended in collagen I solution (Advanced BioMatrix PureCol), and added to 12-well plates. After 4 hours, complete media was then added on top of the well and day 0 pictures were taken. For invasive growth quantification, increase in area occupied by the spheroids between day 0 and day 2 was calculated using FiJi software. For three-dimensional invasion assays, cells were resuspended in an FBS-free bovine collagen I solution at 2.3 mg/mL in a 1:1 proportion to a final concentration of 15,000 cells per 100 μL of matrix and spun down in a 96-well plate. After matrix polymerization, 10% FBS-containing media was added on top. Cells were fixed after 24 hours. The three-dimensional invasion index was calculated counting the number of cells at 50 μm and 100 μm divided by the number of cells at the bottom. Images for three-dimensional invasion were obtained using a Zeiss 710 confocal microscope and cell counting was analyzed using FiJi Software.

Western blot was performed as described previously (9). Briefly, cells were seeded on 6-well plates and 4 days after seeding cell lysates were prepared with RIPA buffer (50 mmol/L TrisHCl pH 7.5, 150 mmol/L NaCl, 1 mmol/L EDTA, 0.1% SDS, 1% Nonidet P40, 1% sodium deoxycholate, 1 mmol/L sodium fluoride, 1 mmol/L sodium orthovanadate, 1 mmol/L beta-glycerophosphate and protease inhibitor cocktail; Roche). The following antibodies were used: PGC1α H300 (Santa Cruz Biotechnology #sc-13067), ERRα (Cell Signaling Technology #13826), ITGβ1 (Cell Signaling Technology #34981S), Caveolin-1 (BD Biosciences, ref: 142610059), β-actin (Cell Signaling Technology #3700S), phospho-cofilin (Cell Signaling Technology #3313), cofilin (Cell Signaling Technology #5175), GAPDH (Cell Signaling Technology #2118), c-MYC (MYC, Cell Signaling Technology #13987S), ITGβ4 (Cell Signaling Technology #14803), ITGα3 (Santa Cruz Biotechnology #sc-374242), ITGα6 (Cell Signaling Technology #3750S), phospho-Src (Life Technologies, ref: 44660G; p-Src Tyr419), and Src 36D10 (Cell Signaling Technology #2109). All were used at a 1:1,000 dilution, except β-actin (1:2,000). Mouse and rabbit secondary antibodies were purchased from Jackson ImmunoResearch. After standard SDS-PAGE and Western blotting techniques, proteins were visualized using the ECL system in the iBright FL1000 Imaging System.

The cytoskeleton phospho-antibody array was performed following Tebu-bio protocol (https://www.tebu-bio.com). Briefly, 5×10^6 induced and noninduced cells were collected and the cell pellet was frozen for further analysis by Tebu-bio services. More than 141 antibodies were present in the screening for phosphorylation rate of main cytoskeleton proteins.

RNA was extracted using NucleoSpin RNA isolation kit from Macherey-Nagel (ref: 740955.240C). For xenograft samples, a TRIzol-based implementation of the NucleoSpin RNA isolation kit protocol was used as reported (24). For all cases, 1 μg of total RNA was used for cDNA synthesis using qScript cDNA Supermix from Quanta (ref: 95048). Quantitative real-time PCR (qRT-PCR) was performed as described previously (9). Universal Probe Library (Roche) primers and probes employed are detailed in Supplementary Table S1. All qRT-PCR data presented were normalized using GAPDH (Hs02758991_g1 from Applied Biosystems).

Chromatin immunoprecipitation

Chromatin immunoprecipitation (ChIP) was performed using the SimpleChIP Enzymatic Chromatin IP Kit (catalog no. 9003, Cell Signaling Technology, Inc). Four million PC3 TRIPZ-Pgc1a cells per immunoprecipitation were grown in 150-mm dishes either with or without 0.5-μg/mL doxycycline during 16 hours. Cells were cross-linked with 37% formaldehyde for 10 minutes at room temperature. Glycine was added to dishes and cells were incubated for 5 minutes at room temperature. Cells were then washed twice with ice-cold PBS and scraped into PBS + PIC. Pelleted cells were lysed and nuclei were harvested following the manufacturer's instructions. Nuclear lysates were digested with micrococcal nuclease for 20 minutes at 37°C and then sonicated in 500-μL aliquots on ice for six pulses of 20 seconds using a Branson sonicator. Cells were held on ice for at least 20 seconds between sonications. Lysates were clarified at 11,000 × *g* for 10 minutes at 4°C, and chromatin was stored at −80°C. HA-Tag polyclonal antibody (Cell Signaling Technology #3724), anti-ERRα antibody (Cell Signaling Technology #13826), and IgG antibody (Cell Signaling Technology #2729) were incubated overnight (4°C) with rotation and protein G magnetic beads were incubated for 2 hours (4°C). Washes and elution of chromatin were performed following manufacturer's instructions. DNA quantification was carried out using a Viia7 Real-Time PCR System (Applied Biosystems) with SYBR Green reagents and primers that amplify a *PGC1A* binding region to *MYC* promoter (shown in Supplementary Table S2).

Bioinformatic analysis and statistics

Bioinformatic analysis containing patient data was performed using the web-based interface Cancertool (25).

For each available patient dataset, the values of PGC1α-ERRα signature were calculated from the average of the expression signal of those genes that are part of the aforementioned signature (*ACACB*, *ACSL4*, *ATP1B1*, *GSTM4*, *ISCU*, *LAMB2*, *NNT*, *PPIC*, *SOD2*, *SUCLA2*). In the case of PPARGC1A/NRIP1 ratio, we calculated the average expression value of PPARGC1A, and, as values are $\log_2$ scaled, subtracted the average expression value of NRIP1. R software (https://cran.r-project.org/), version 3.5.1, has been used for these calculations, together with ggplot2 package (https://cran.r-project.org/web/packages/ggplot2) to perform the corresponding graphs.

Individual gene expression patters in patient dataset, as well as pairwise correlation information, can be visualized in the Cancertool interface.

The differential gene expression analysis driven by PGC1α in PC3 cells can be obtained from GEO with reference GSE75193.

In addition, pathway and network enrichment analyses of the significantly regulated genes from GSE75193 (Supplementary Table S3) were performed using MetaCore from GeneGo Inc (https://portal.genego.com/).

No statistical method was used to predetermine sample size. The experiments were not randomized. The investigators were not blinded to allocation during experiments and outcome

assessment. *n* values represent the number of independent experiments performed, the number of individual mice, or patient specimens. For each independent *in vitro* experiment, normal distribution was assumed, and one-sample *t* test was applied for one-component comparisons with control and Student *t* test for two-component comparisons. For *in vivo* experiments, a nonparametric Mann–Whitney exact test was used. Two-tailed statistical analysis was applied for experimental design without predicted result, and one-tailed for validation or hypothesis-driven experiments. The confidence level used for all the statistical analyses was of 95% (alpha value = 0.05). GraphPad Prism 8 software was used for statistical calculations.

Results

To address the role of PGC1α in the regulation of prostate cancer features beyond proliferation (17), we carried out a comprehensive evaluation of phenotypes associated to cancer aggressiveness, based on an inducible system reported previously (17). Interestingly, Pgc1α expression elicited a remarkable reduction in the migratory capacity of PC3 and DU145 prostate cancer cells in transwell assays (Fig. 1A; Supplementary Fig. S1A). A similar effect was achieved in Matrigel-coated transwell assays as a measure of invasion (Fig. 1B; Supplementary Fig. S1B). To further characterize the regulation of invasive properties by PGC1α, we applied two complementary assays in both cell lines. On the one hand, we performed three-dimensional invasion assays. We quantified the number of cells invading at 50 μm and/or 100 μm of distance from the bottom of the plate. The results showed a profound decrease in cells with invasive capacity upon Pgc1α induction (Fig. 1C; Supplementary Fig. S1C and S1D). On the other hand, we generated spheroids using the hanging drop method to measure the invasive growth. The results corroborated that the expression of the coregulator inhibits the invasive capacity of prostate cancer cells (Fig. 1D; Supplementary Fig. S1E). Of note, this phenotype was observed at time points where proliferation was not significantly influenced by Pgc1α or by the addition of doxycycline (Supplementary Fig. S1F–S1I; ref. 17). Overall, our results show that beyond the antiproliferative capacity of PGC1α in prostate cancer, the transcriptional coregulator elicits a robust anti-invasive phenotype.

The regulation of cell migration and invasion is intertwined with cell morphology and adhesion (19). Hence, we characterized the effects of PGC1α on these parameters. The expression of the coregulator in PC3 cells was associated with a remarkable elevation in cell area, with loss of stress fibers and with a modest increase in cell adhesion to collagen I (Fig. 1E and **F**; Supplementary Fig. S1J). Importantly, Pgc1α induction in subcutaneous xenografts of PC3 cells confirmed the antitumoral activity of this gene and its impact on prostate cancer cell size *in vivo* (Fig. 1G; Supplementary Fig. S1K–S1M).

We next focused on the molecular alterations underlying the activity of PGC1α. In a previous study, we analyzed a gene expression analysis in PC3 cells upon induction of Pgc1α (Fig. 1; GSE75193; ref. 17). We sought to extend the analysis of this microarray by taking advantage of bioinformatic tools, such as Metacore (https://clarivate.com/products/metacore/) and Cancertool (25) that enable cancer researchers to perform various functional enrichment analyses. Because functional enrichment allows the integration of larger sets of data to identify underlying molecular and functional alterations, we focused our analyses on all genes whose expression was altered with a significant *P* value in the transcriptomics analysis (regardless of the P_{adj} value). This led to 1,347 upregulated and 990 downregulated unique gene IDs (Supplementary Table S3). Strikingly, functional enrichment of the downregulated genes revealed a significant alteration in cytoskeleton organization, migration, adhesion, and integrin and Rho signaling (Fig. 2A; Supplementary Fig. S2A; Supplementary Tables S4 and S5). Of note, we also identified other pathways with reported activities in the regulation of invasion, such as p27, FAS, and RAC, although their prevalence in the analysis and their documented association to this phenotype were minor (26–29). In line with our previous study (17), the enrichment analysis of the genes upregulated upon Pgc1α expression confirmed a significant alteration of catabolic pathways (Supplementary Table S6). We focused our attention in the Metacore analysis of downregulated genes. The results revealed a remarkable alteration in cytoskeletal remodeling upon PGC1α modulation in prostate cancer cells, illustrated by processes regulated by Rho kinase (ROCK). The axes containing ROCK-LIM kinase (LIMK)-Cofilin and ROCK-myosin light chain (MLC) are two key signaling pathways that regulate cytoskeletal remodeling downstream of the monomeric G protein Rho and integrin signaling (30). The immunostaining and quantification of phosphorylated myosin-light chain 2 (p-MLC2) revealed a significant reduction in this parameter in Pgc1α-expressing PC3 cells (Fig. 2B). This result supports the notion that loss of PGC1α in prostate cancer cells results in changes in the actin–myosin cytoskeleton that are associated with the acquisition of invasive properties. To ascertain which signaling pathways were modulated and affecting cytoskeleton organization upon Pgc1α expression, we carried out a cytoskeleton phospho-antibody array (Supplementary Table S7). The phosphorylation of Src protein was among the most prominently reduced in the analysis (Supplementary Fig. S2B). We confirmed this result by Western blot analysis, both *in vitro* and *in vivo*, together with the reduction in cofilin phosphorylation, the final effector of actin filament polymerization downstream Src (Fig. 2C and **D**; Supplementary Fig. S2C and S2D).

Integrins are upstream regulators of the cytoskeleton with well-documented involvement in cancer aggressiveness (19, 31, 32). The bioinformatics analysis of PGC1α-downregulated genes indicated an altered integrin signaling (Fig. 2A; Supplementary Fig. S2A), which would be consistent with the reduction in Src, MLC2, and cofilin phosphorylation. This, together with the fact that PGC1α controls integrin expression in melanoma (16), prompted us to evaluate integrin expression in our experimental systems. Interestingly, the levels of various integrins and caveolin-1 (CAV1, but not CAV2) were robustly reduced at protein and mRNA levels upon Pgc1α induction, an event that was not influenced by doxycycline treatment (Fig. 2E; Supplementary Fig. S2E–S2I). Next, we analyzed extracts from xenografts in which Pgc1α expression was activated (Fig. 1G). The Western blot and quantitative qRT-PCR analysis corroborated the alterations elicited by the coactivator *in vivo* (Fig. 2F; Supplementary Fig. S2J and S2K). Our results suggest that PGC1α controls a transcriptional program that results in the alteration of cytoskeleton organization with the concomitant reduction in integrin expression, an event that is consistent with the observed reduction in migratory and invasive properties of prostate cancer cells.

We then asked which effector of PGC1α could contribute to the negative regulation of invasive properties. Inhibitors of

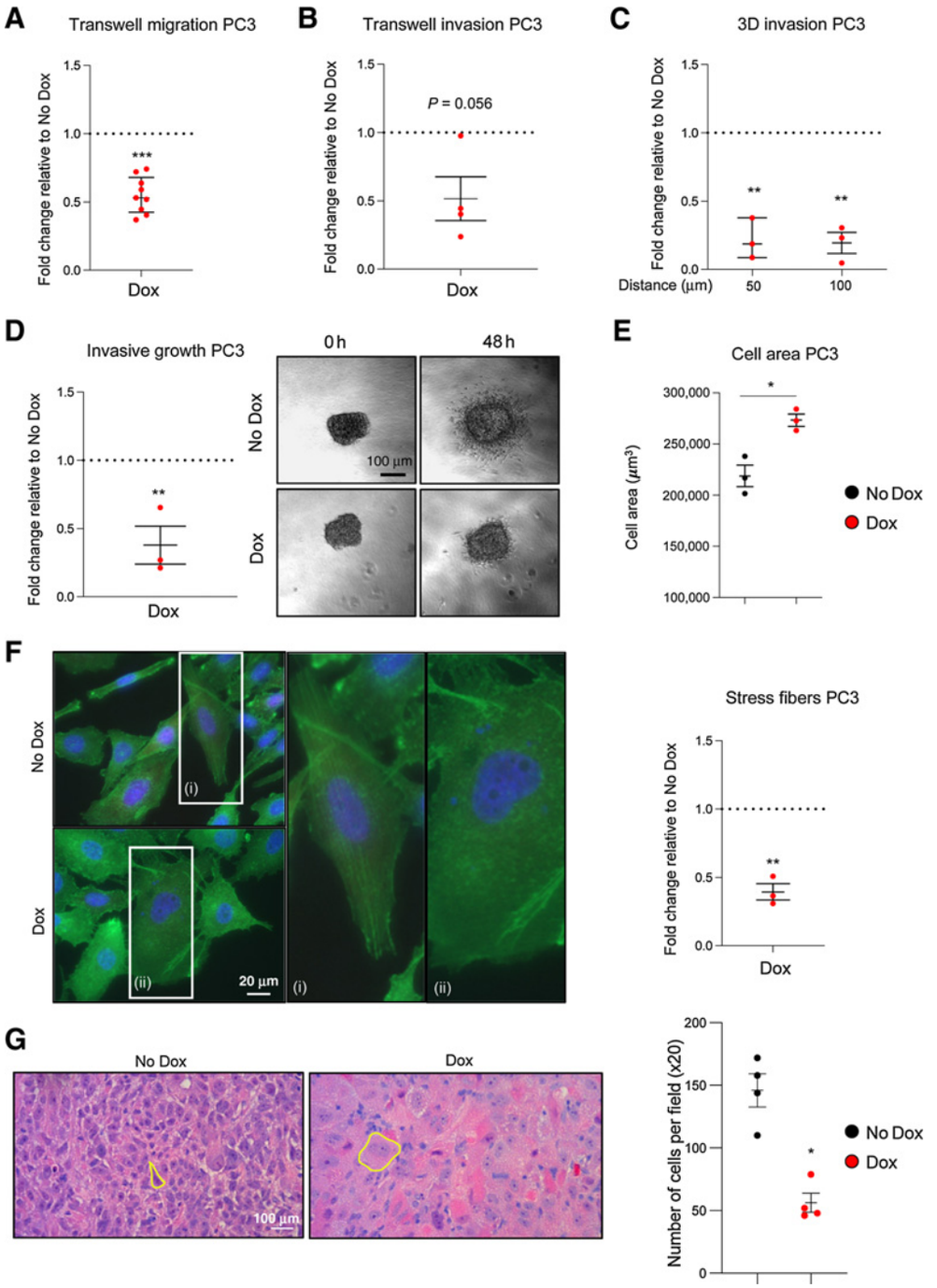

Figure 1.

PGC1α expression impacts on invasive properties of prostate cancer *in vitro* and *in vivo*. **A** and **B,** Effect of Pgc1α expression on transwell migration ($n = 9$ independent experiments; **A**) and on transwell invasion ($n = 4$ independent experiments; **B**) of PC3 cells. **C** and **D,** Effect of Pgc1α expression on 3D invasion ($n = 3$ independent experiments; **C**) and invasive growth ($n = 3$ independent experiments; **D**) of PC3 cells. **D,** Right, one representative experiment of invasive growth; left, the quantification. **E** and **F,** Quantification of changes in cell area (**E**) and stress fibers (**F**) content upon Pgc1α expression in PC3 cells *in vitro* ($n = 3$ independent experiments). **F,** Representative phalloidin staining of nonexpressing (No Dox) and Pgc1α-expressing PC3 cells (left) and quantification (right). **G,** Quantification of changes in cell area upon Pgc1α expression in PC3 cells *in vivo*. Left, representative hematoxylin and eosin staining of nonexpressing and Pgc1α-expressing xenograft samples ($n = 4$ tumors each condition, No Dox and Dox). Yellow line outlines cell surface. Right, the quantification of number of cells per field. Dox, doxycycline, Pgc1α-induced conditions; No Dox, Pgc1α nonexpressing conditions. In **A, B, C, D,** and **F,** data are represented as fold change relative to No Dox condition depicted by a dotted line. Error bars, SEM. Statistic tests: one-sample *t* test with a hypothetical value of 1 (**A**, **B**, **C**, **D**, and **F**), two-tailed Student *t* test (**E**), and one-tailed Mann–Whitney U test (**G**). *, $P < 0.05$; **, $P < 0.01$; ***, $P < 0.001$.

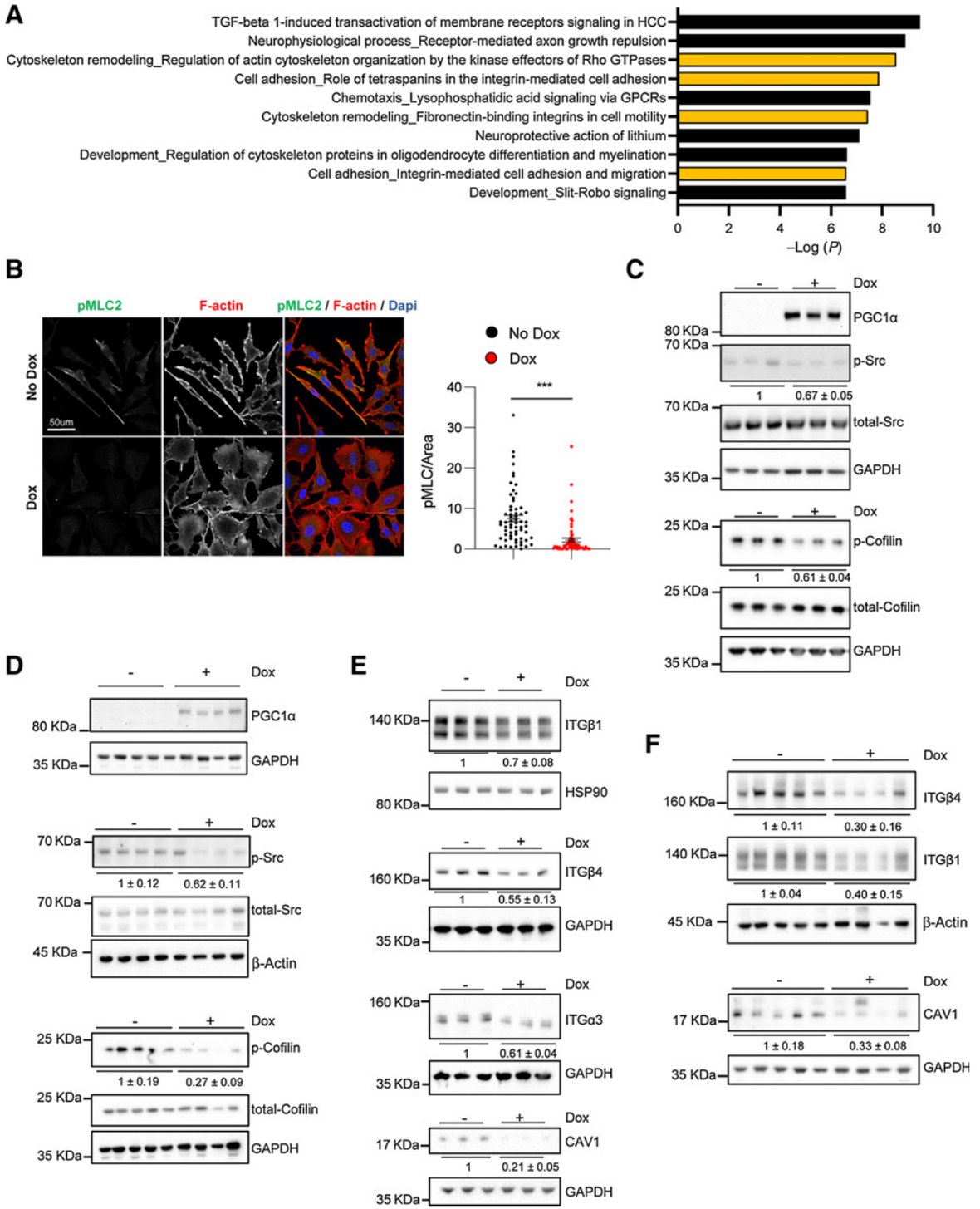

Figure 2.

PGC1α expression modulates integrin signaling of prostate cancer *in vitro* and *in vivo*. **A,** Metacore enrichment analysis of the transcriptional program downregulated by PGC1α in PC3 cells. **B,** Effect of Pgc1α expression on the phosphorylation of MLC protein in PC3 cells. Left, representative images of immunofluorescence staining using p-MLC antibodies. Right, quantification of p-MLC per cell area ($n = 3$ independent experiments). **C** and **D,** Representative Western blot analysis of the effect of Pgc1α on cofilin and Src phosphorylation in PC3 cells (**C**) and xenograft samples (**D**). Representative Western blot analysis of the effect of Pgc1α on ITGβ1, ITGβ4, ITGα3, and CAV1 in PC3 cells ($n = 3$; independent experiments; **E**) and xenograft samples ($n = 4$–5 tumors; **F**). Dox, doxycycline, Pgc1α-induced conditions; No Dox, Pgc1α-nonexpressing conditions. Error bars, SEM. Western blot quantifications are presented as ± SEM. Statistic tests: two-tailed Student *t* test (**B**). ***, $P < 0.001$.

differentiation are responsible for integrin repression in melanoma (16). We ruled out the potential contribution of ID2-4 to our phenotype, because their expression was not upregulated upon induction of the coactivator (Supplementary Fig. S3A). Then, we applied promoter enrichment analysis (25) to the list of Pgc1α-repressed genes. Strikingly, the results revealed a significant enrichment in MYC within the promoters of the downregulated genes ($P = 8.5e\text{-}19$; Fig. 3A; Supplementary Tables S3 and S8). We studied the impact of PGC1α on the expression of MYC and observed that induction of the coregulator elicited a consistent decrease in MYC expression in prostate cancer cells in a doxycycline-independent manner (Fig. 3B; Supplementary Fig. S3B and S3C). Importantly, the effect was fully recapitulated at the transcriptional level. In addition, the analysis of previously reported targets or genes contained in the promoter analysis confirmed the reduction in MYC-dependent transcriptional program in the aforementioned conditions (Fig. 3C). We took advantage of our Pgc1α-inducible xenograft analysis to further demonstrate that the reduction in MYC expression and function was not an artifact of *in vitro* assays (Fig. 3D and **E**; Supplementary Fig. S3D). These

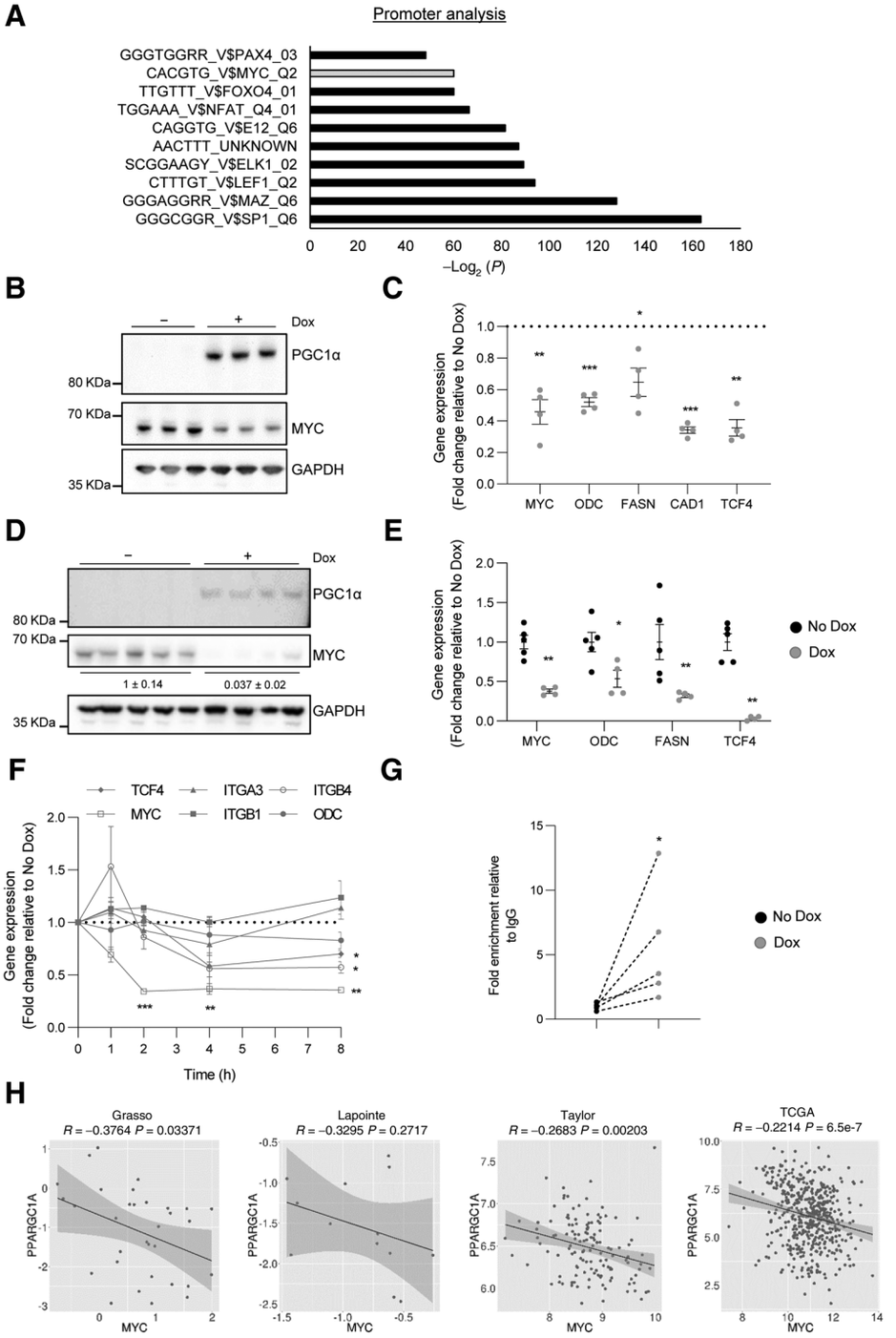

Figure 3.

PGC1α regulates c-Myc expression in prostate cancer. **A,** Promoter enrichment analysis of the PGC1α transcriptional program in PC3 cells. **B,** Effect of Pgc1α expression on c-Myc protein levels in PC3 cells ($n = 3$ independent experiments). **C,** Quantification of *MYC* gene expression and its target genes *ODC, FASN, CAD1,* and *TCF4* by qRT-PCR upon Pgc1α expression in PC3 cells ($n = 4$ independent experiments). Data are represented as fold change relative to No Dox, depicted as a dotted line. **D,** Effect of Pgc1α expression on c-Myc protein levels in xenograft samples ($n = 5$ No Dox tumors; $n = 4$ Dox tumors). **E,** Quantification of *MYC* gene expression (and its target genes) by qRT-PCR in xenograft samples cells ($n = 5$ No dox tumors; $n = 4$ Dox tumors). **F,** qRT-PCR gene expression analysis of MYC, TCF4, ITGB4, ITGB1, and ITGA3 upon short acute induction of Pgc1α expression (1, 2, 4, and 8 hours of doxycycline treatment) in PC3 cells. Data are represented as fold change relative to No Dox, depicted as a dotted line. **G,** ChIP of exogenous Pgc1α on MYC promoter in PC3 Pgc1α cells after induction with 0.5-μg/mL doxycycline for 16 hours ($n = 5$). Final data were normalized to IgG (negative immunoprecipitation control) and to No Dox condition. **H,** Correlation analysis between PGC1A and MYC expression in primary tumor specimens of different prostate can datasets. Sample sizes: Grasso, $n = 45$; Lapointe, $n = 13$; Taylor, $n = 131$; and TCGA provisional, $n = 495$. Dox, doxycycline, Pgc1α-induced conditions; No Dox, Pgc1α-nonexpressing conditions. Error bars, SEM. Western blot quantifications are presented as ± SEM. Statistic tests: one-sample *t* test with a hypothetical value of 1 (**C** and **F**), one-tailed Student *t* test (**G**), one-tailed Mann–Whitney U test (**E**), Spearman correlation *R* (**H**). *, $P < 0.05$; **, $P < 0.01$; ***, $P < 0.001$.

results suggest that MYC repression is upstream of the molecular and cellular alterations elicited by PGC1α associated to prostate cancer invasion. We validated this notion by two different means. On the one hand, a time course experiment upon PGC1α induction showed that MYC repression is prior to the reduction of its targets and integrin gene expression (Fig. 3F; Supplementary Fig. S3E–S3G). On the other hand, MYC silencing with a validated shRNA (33, 34) recapitulated the phenotype of Pgc1a expression in cell area, p-MLC2, and invasive growth (Supplementary Fig. S3H–S3L).

The rapid repression in MYC mRNA levels prompted us to evaluate whether PGC1α could exert a direct action on MYC promoter. To this end, we performed ChIP analysis in Pgc1α-inducible PC3 cells with anti-HA antibody to immunoprecipitate ectopic tagged Pgc1α. The ChIP analysis confirmed that the coregulator is bound to MYC promoter (Fig. 3G), thus suggesting that PGC1α represses MYC expression in prostate cancer. We next sought to ascertain whether the unprecedented regulation of MYC by PGC1α in prostate cancer could be recapitulated in human specimens. We interrogated 5 prostate cancer datasets (25, 35–37) and, in agreement with our molecular and mechanistic data, *PGC1A* expression was inversely correlated with *MYC* mRNA levels in primary tumors from the majority (four out of five) of datasets analyzed (Fig. 3H; Supplementary Fig. S3M).

Our previous studies demonstrated that the antiproliferative activity of PGC1α in prostate cancer is dependent on its interaction with ERRα (17). To ascertain the requirement of ERRα for the anti-invasive activity of PGC1α, we engineered Pgc1α-inducible prostate cancer cells in which *ESRRA* was deleted using CRISPR/Cas9. ERRα expression was undetectable in PC3 cells in which *ESRRA* was deleted with two independent sgRNAs (sgERRα#1, sgERRα#2; Fig. 4A). *ESRRA* deletion abolished the induction of target genes of the transcription factor upon induction of Pgc1α, corroborating the functionality of the genetic system (Supplementary Fig. S4A). Of note, we did not recapitulate the regulation of *ESRRA* by *PGC1A* observed *in vitro* (Fig. 4A) in correlative human transcriptomics analyses, suggesting that more complex ERRα-regulatory cues might operate in human disease (Supplementary Fig. S4B). In line with our previous study (17), *ESRRA* deletion hampered the growth-suppressive activity of Pgc1α, rendering PC3 cells insensitive to the action of the coregulator (Fig. 4B). Strikingly, *ESRRA* deletion also abolished the effect of Pgc1α on invasive properties and cell morphology at time points prior to the reduction in cell proliferation, thus demonstrating that the regulation of invasion by the coregulator is exquisitely dependent upon its interaction with ERRα (Fig. 4C and **D**; Supplementary Fig. S4C and S4D). The morphologic changes and growth-suppressive phenotype elicited by Pgc1α were also absent in tumors in which *ESRRA* was deleted (Fig. 4E; Supplementary Fig. S4E–S4G). It is worth noting that despite the requirement of ERRα for the tumor-suppressive activity of PGC1α, deletion of the nuclear receptor alone negatively influenced the establishment of tumors, suggesting that additional functions of ERRα may be required for the first stages of tumor establishment (Supplementary Fig. S4H).

We next extended our analysis of ERRα dependency to the reported molecular alterations. Our results showed that *ESRRA* deletion abrogated the reduction in protein and/or mRNA levels of MYC, MYC targets, integrins, CAV1, as well as the reduced phosphorylation of Src and cofilin (Fig. 5A and B; Supplementary Fig. S5A and S5B). Moreover, *ESRRA*-ablated tumors exhibited unperturbed MYC, integrin, and CAV1 expression, as well as unchanged Src and cofilin phosphorylation upon Pgc1α expression (Fig. 5C and D; Supplementary Fig. S5C). All these data are in line with the association of ERRα to MYC promoter in Pgc1α-expressing PC3 cells (Supplementary Fig. S5D).

Because we have observed a robust inverse correlation between *PGC1A* and *MYC* expression in various prostate cancer datasets, we asked whether the dependency on ERRα could be recapitulated in this setting. To this end, we carried out two independent approaches in datasets of patients with prostate cancer. On the one hand, we inferred ERRα canonical activity based on the equilibrium between its main coactivators (*PGC1A*) and corepressors (*NRIP1*). We calculated the ratio of abundance of *PGC1A* and *NRIP1* transcript (*PGC1A*/*NRIP1*), which provided an estimation of ERRα canonical activity toward its targets, as confirmed through the analysis of *ACACB* and *LAMB2* expression (Supplementary Fig. S6A). In line with our mechanistic analysis, ERRα activity but not ERRα itself, was consistently and inversely correlated with *MYC* in various prostate cancer datasets (Supplementary Fig. S6B and S6C). On the other hand, we took advantage from a prognostic PGC1α-ERRα signature that we generated previously (17). This signature was composed of 10 genes that were (i) regulated by PGC1α *in vitro*, (ii) predicted to be ERRα targets, and (iii) correlated with *PGC1A* in prostate cancer datasets. In full support of our data, this PGC1α-ERRα activity signature was inversely correlated with *MYC* expression in various datasets of patients with prostate cancer (Fig. 5E; Supplementary Fig. S6D).

Overall, our results provide solid evidence of the anti-invasive activity of the PGC1α–ERRα transcriptional axis in prostate cancer.

Discussion

Metabolic deregulation is a hallmark of cancer (2) and encompasses a variety of biochemical routes, which must be coordinated to result in a phenotypic change. We postulated in the past that this strict requirement for coordination could unveil novel cancer genes. By focusing on transcriptional coregulators that control the expression of an ample set of metabolic genes, we discovered the predominant perturbation of PGC1α in prostate cancer (7, 17). This metabolic regulator orchestrates the activation of catabolic and antioxidant pathways at the expense of anabolism (8). Interestingly, the contribution of PGC1α to cancer biology is complex. Elegant studies have reported a role of this coregulator: (i) promoting aggressiveness of breast, pancreatic, and gastric tumors; cholangiocarcinoma; glioma; and melanoma (10–14, 38–40), and (ii) suppressing cancer aggressiveness in prostate, kidney tumors, and melanoma (9, 15–18). Moreover, the expression of this coregulator is associated with the efficacy of anticancer therapies (10, 11, 14, 15, 41, 42).

PGC1α exhibits an activity that is dependent on the tumor type, ranging from tumor suppressor to advantageous for cancer cells (7). This coactivator is required for the activity of pancreatic cancer stem cells (13) and for the survival of breast cancer cells in circulation (12). In melanoma, the metabolic activity of PGC1α promotes cell proliferation, whereas the nonmetabolic function opposes metastatic dissemination (10, 11, 16).This study together with reports by us and others demonstrates that PGC1α suppresses proliferation and invasion in prostate cancer through

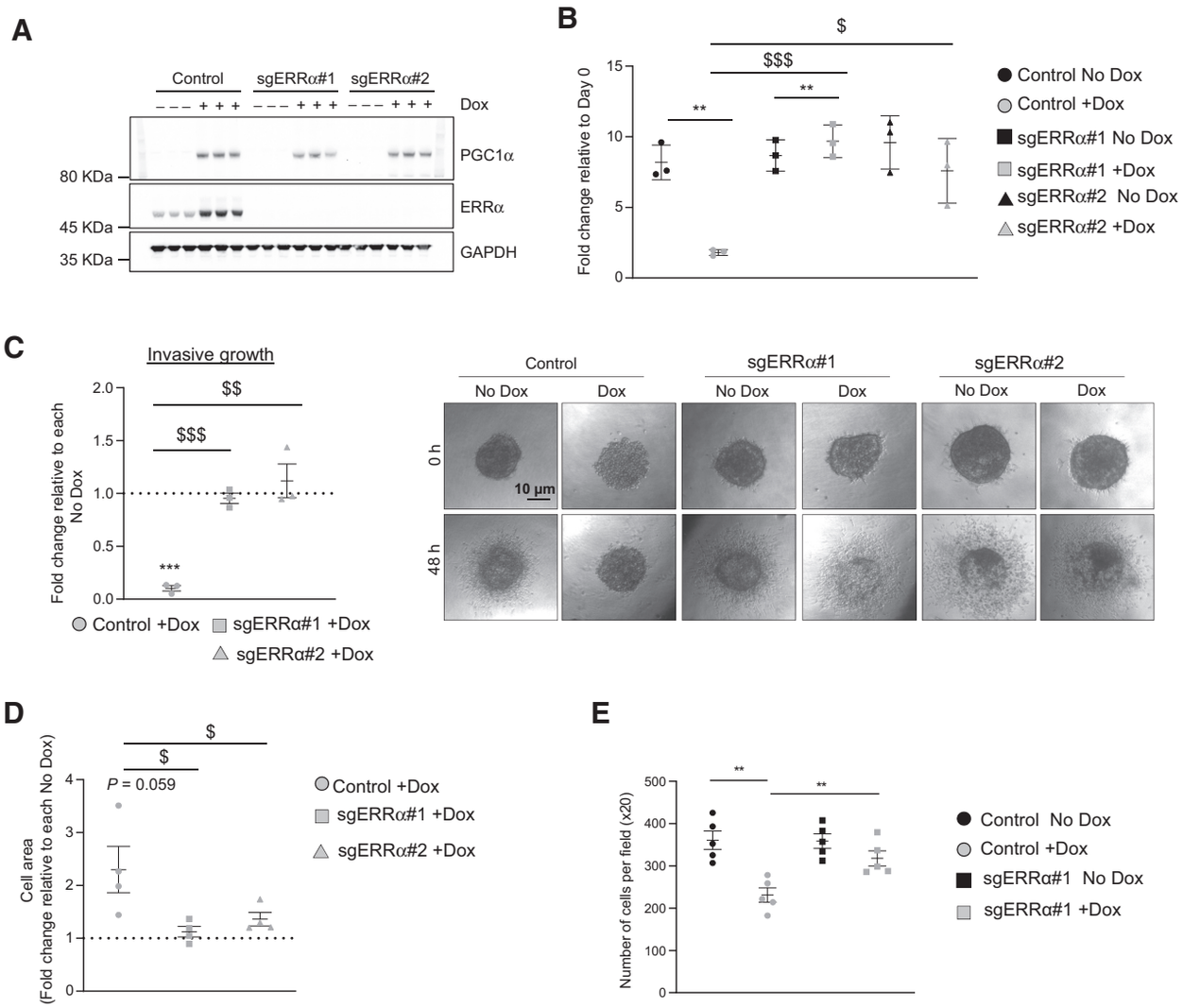

Figure 4.

ERRα deletion mediates the effect of Pgc1α on invasive properties and morphology of prostate cancer *in vitro* and *in vivo*. **A,** Representative experiment of ERRα expression in PC3 Pgc1α cells after treatment with 0.5-μg/mL doxycycline (Dox; $n = 3$; independent experiments). **B,** Relative cell number quantification upon ERRα deletion (sgERRα#1 and sgERRα#2) in PC3 Pgc1α expressing and nonexpressing cells. Data are represented as cell number at day 6 relative to day 0 ($n = 3$, independent experiments). **C,** Effect of ERRα deletion in invasive growth upon Pgc1α expression ($n = 3$ independent experiments). One representative spheroid image of each condition is shown out of three biological replicates. **D,** Quantification of cell area by phalloidin staining after ERRα deletion alone or in combination with Pgc1α expression ($n = 4$ independent experiments) in PC3 cells. **E,** Effect of ERRα deletion alone or in combination of Pgc1α on the cell content and size in xenograft samples ($n = 5$ per condition). The number of cells per field is an approximate representation of cell area. Dox, doxycycline, Pgc1α-induced conditions; No Dox, Pgc1α nonexpressing conditions. Error bars, SEM. Dotted line, No Dox condition. Statistic tests: paired Student *t* test between Control −Dox and +Dox conditions (**B**), unpaired Student *t* test between +Dox control and sg conditions (**B**), one sample *t* test with a hypothetical value of 1 (**C** and **D**), and one-tailed Mann–Whitney *U* test (**E**). $, $P < 0.05$; **/$$, $P < 0.01$; ***/$$$, $P < 0.001$. Asterisks indicate statistical difference between No Dox and Dox conditions (**B, C,** and **E**) and dollar symbols indicate statistical difference between Control Dox and sgERRα#1/sgERRα#2 Dox (**B** and **D**).

presumably distinct molecular pathways emanating from the regulation of ERRα, consistent with its tumor- and metastasis-suppressive function (Fig. 6; refs. 17, 18). Our results mirror the anti-invasive activity of the coregulator in melanoma, whereas proliferation is regulated in opposite sense in both tumor types. This apparent discrepancy could be associated to the tissue-specific molecular cues that drive these tumors or the distinct nutrient and metabolic pathways that sustain their growth.

Cancer cell proliferation imposes tremendous pressure to meet the bioenergetics demands and to generate sufficient biomolecules to build new cells. We now possess a more comprehensive view of the metabolic deregulations that sustain or accompany cancer cell proliferation (43). However, beyond the relevance of cell proliferation in cancer, tumor cells need to acquire additional capacities that account for the clinical progression of the disease. The process of metastasis

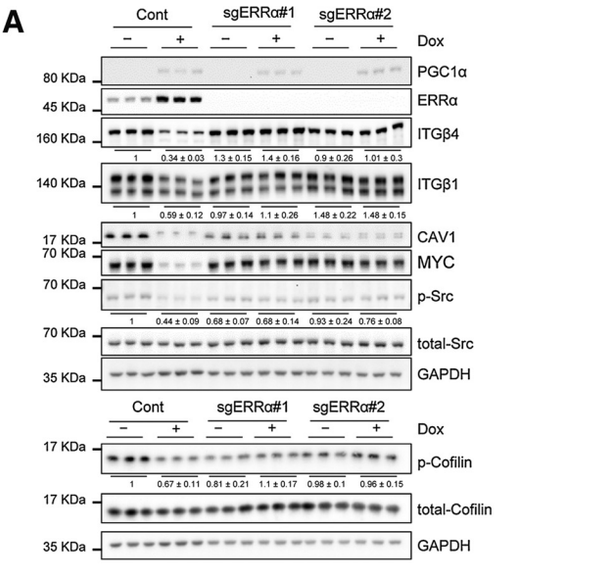

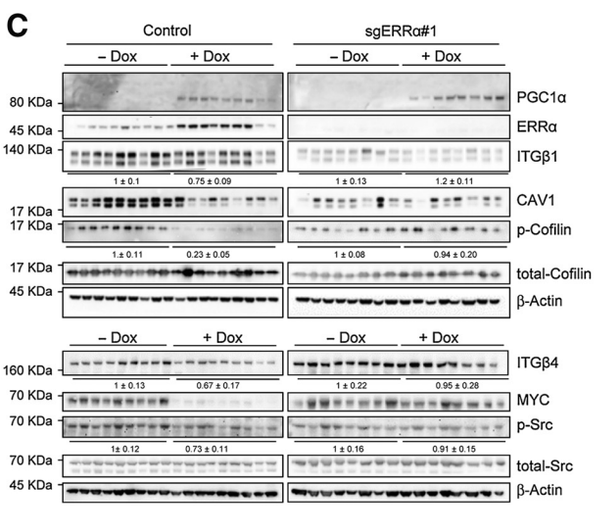

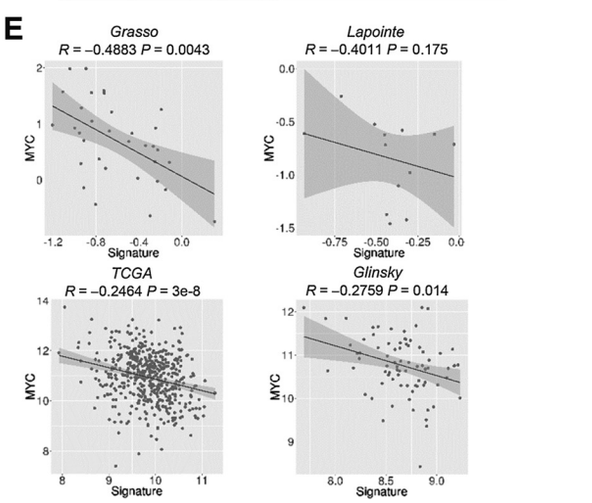

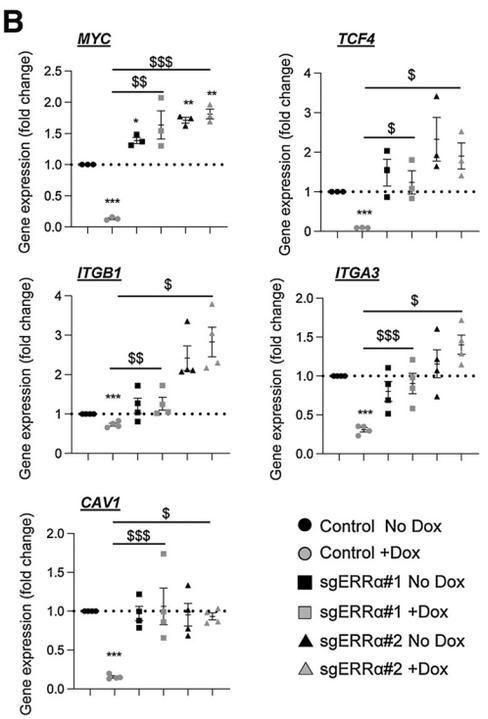

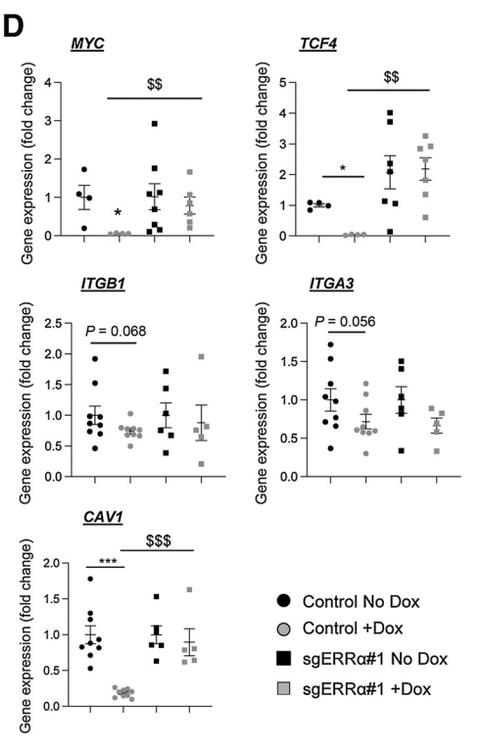

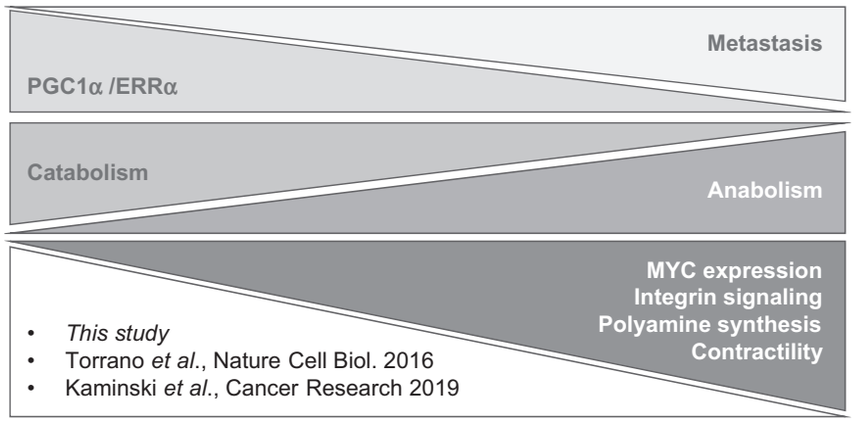

Figure 6.
Schematic summary of the main findings. Torrano et al. (17); Kaminski et al. (18).

is the main cause of mortality in cancer and only partly depends on cell proliferation, as it requires angiogenesis, intravasation, survival in circulation, extravasation, and resuming cell growth in a distant organ (44). Our perspective around the contribution of metabolic regulators to the acquisition of these features is limited. An exciting possibility stems from the notion that factors that control metabolic programs would also regulate molecular cues associated to cancer cell dissemination.

Little is known about the activities of PGC1α in cancer beyond proliferation. This coregulator inhibits dissemination in melanoma through the regulation of ID2-TCF4-Integrins (16). In gastric cancer, a recent report suggests that PGC1α upregulation supports metastasis though the regulation of SNAI1 (38). Interestingly, none of these effects are ascribed to the regulation of its main transcriptional partner, ERRα. Instead, we demonstrate that the PGC1α-ERRα transcriptional axis in prostate cancer accounts for the invasive phenotype. We demonstrate that PGC1α/ERRα status influences signaling pathways that are important for the regulation of cytoskeletal remodeling. In turn, changes in pathways related to integrin and ROCK signaling provide a feasible explanation for the anti-invasive effects of the coregulator. Interestingly, the set of genes inhibited in PGC1α-expressing cells that relate to cytoskeletal remodeling is enriched in MYC promoter–binding sites. These data are consistent with the notion that PGC1α/ERRα represses MYC expression and that silencing of this transcription factor partly phenocopies the effect of PGC1α (18).

Similar to PGC1α, ERRα has opposing effects in different tumor types (7). Interestingly, we show that this nuclear receptor is required for the tumor suppressive activity of PGC1α, whereas its deletion delays tumor onset in immunocompromised mice independently of the induction of PGC1α. Our results could be explained by the differential requirement of basal ERRα activity for the establishment of tumors (homing and the initial engagement of cell proliferation *in vivo*) versus the proliferation and invasion in later stages. Similar results were reported for LKB1, which is required for the bypass of anoikis and the survival of tumor cells in conditions of energetic stress, despite its tumor suppressive nature in established tumors (45, 46).

ERRα functions predominantly as a transcriptional activator and is rarely reported to repress the expression of target genes (47). However, recent studies demonstrate that a subset of the genes identified by ERRα ChIP-seq is repressed by the nuclear receptor (48). In this sense, our results demonstrating that PGC1α/ERRα inhibits the expression of *MYC* broaden the spectrum of repressed genes by the protein complex. Interestingly, work by the group of Dr. Frederic Bost (French Institute of Health and Medical Research, Inserm, Paris, France) reports that PGC1α regulates an alternative branch of metabolism (polyamine biosynthesis) through the ERRα-dependent repression of MYC-ODC1 (18), thus opening new molecular avenues connecting this coactivator to metabolic pathways that coordinate proliferation and invasion.

In summary, our study together with recent reports (18) demonstrates that PGC1α/ERRα coordinately controls proliferative and invasive features in prostate cancer, thus providing a feasible explanation for its robust clinical association to biochemical recurrence and metastasis.

Figure 5.
ERRα mediates the effect of Pgc1α on integrin signaling and MYC expression *in vitro* and *in vivo*. **A,** Representative Western blot of the effect of ERRα deletion alone or in combination with Pgc1α expression on ITGβ1, ITGβ4, CAV1, and MYC protein expression as well as on cofilin and Src phosphorylation in PC3 cells ($n = 3$; independent experiments). **B,** Effect of ERRα deletion alone or in combination with Pgc1α expression in the gene expression (qRT-PCR) of MYC, TCF4, ITGB1, ITGA3, and CAV1 ($n = 4$ independent experiments) in PC3 cells. Data are represented by fold change relative to Control No Dox condition that is depicted by a dotted line. **C,** Effect of ERRα deletion alone or in combination with Pgc1α expression on ITGβ1, ITGβ4, CAV1, and MYC protein expression as well as on cofilin and Src phosphorylation in xenograft samples (Control No Dox, $n = 9$ tumors; Control + Dox, $n = 9$ tumors; sgERRα#1 –Dox, $n = 8$ tumors; sgERRα#2 +Dox, $n = 8$ tumors). **D,** Effect of ERRα deletion alone or in combination with Pgc1α expression MYC, TCF4, ITGB1, ITGA3, and CAV1 gene expression analyzed by qRT-PCR in xenograft samples. (Control No Dox, $n = 4$–9 tumors; Control +Dox, $n = 4$–9 tumors; sgERRα#1 No Dox, $n = 6$–8 tumors; sgERRα#2 +Dox, $n = 5$–6 tumors). **E,** Correlation analysis between MYC and the PGC1α-ERRα transcriptional signature in primary tumor specimens of different prostate cancer datasets. Each dot corresponds to a patient. Sample sizes: Grasso, $n = 45$; Lapointe, $n = 13$; Glinsky, $n = 78$; and TCGA provisional, $n = 495$. Dox, doxycycline, Pgc1α-induced conditions; No dox, Pgc1α nonexpressing conditions. Error bars, SEM. Western blot quantifications are presented as ± SEM. Statistic tests: one sample *t* test (**B**), unpaired *t* test (**B** and **D**), and Spearman correlation *R* (**E**). */$, $P < 0.05$; **/$$, $P < 0.01$; ***/$$$, $P < 0.001$. Asterisks indicate statistical difference between Control No Dox and the rest of the conditions and dollar symbols indicate statistical difference between Control Dox and sgERRα#1/sgERRα#2 Dox.

Disclosure of Potential Conflicts of Interest

No potential conflicts of interest were disclosed.

Authors' Contributions

Conception and design: L. Valcarcel-Jimenez, V. Torrano, A. Carracedo
Development of methodology: L. Valcarcel-Jimenez, E. Crosas-Molist, V. Sanz-Moreno, V. Torrano, A. Carracedo
Acquisition of data (provided animals, acquired and managed patients, provided facilities, etc.): L. Valcarcel-Jimenez, A. Macchia, E. Crosas-Molist, A. Schaub-Clerigué, L. Camacho, N. Martín-Martín, P. Cicogna, C. Viera-Bardón, S. Fernández-Ruiz, I. Hermanova, I. Astobiza, A.R. Cortazar, J. Corres-Mendizabal
Analysis and interpretation of data (e.g., statistical analysis, biostatistics, computational analysis): L. Valcarcel-Jimenez, A. Macchia, N. Martín-Martín, I. Rodriguez-Hernandez, A.R. Cortazar, V. Sanz-Moreno, V. Torrano, A. Carracedo
Writing, review, and/or revision of the manuscript: L. Valcarcel-Jimenez, I. Hermanova, V. Torrano, A. Carracedo
Administrative, technical, or material support (i.e., reporting or organizing data, constructing databases): S. Fernández-Ruiz, I. Astobiza, A.R. Cortazar
Study supervision: V. Torrano, A. Carracedo
Other (cosupervision of L. Camacho's work): A. Gomez-Muñoz

Acknowledgments

Apologies to those whose related publications were not cited because of space limitations. We are grateful to the Carracedo lab for valuable input and to Dr. James D. Sutherland for technical advice. V. Torrano is funded by Fundación Vasca de Innovación e Investigación Sanitarias, BIOEF (BIO15/CA/052), the AECC J.P. Bizkaia and the Basque Department of Health (2016111109), and the MINECO RTI2018-097267-B-I00. The work of A. Carracedo is supported by the Basque Department of Industry, Tourism and Trade (Elkartek) and the Department of Education (IKERTALDE IT1106-16, also participated by A. Gomez-Muñoz), the BBVA Foundation, the MINECO (SAF2016-79381-R (FEDER/EU), Severo Ochoa Excellence Accreditation SEV-2016-0644-18-1, Excellence Networks SAF2016-81975-REDT), European Training Networks Project (H2020-MSCA-ITN-308 2016 721532), the AECC (IDEAS175CARR, GCTRA18006CARR), La Caixa Foundation (HR17-00094), and the European Research Council (Starting Grant 336343, PoC 754627). CIBERONC was cofunded with FEDER funds and funded by ISCIII. L. Valcarcel-Jimenez and A. Schaub-Clerigué were funded by a Basque Government predoctoral grant, A. Macchia was funded by a FPI predoctoral fellowship from MINECO (PRE2018-083607), and C. Viera-Bardón was funded by a predoctoral grant of the UPV/EHU. I. Hermanova was funded by the Juan de la Cierva program of the MINECO. V. Sanz-Moreno was supported by Cancer Research UK (CRUK) C33043/A12065 and C33043/A24478 (to V. Sanz-Moreno and E. Crosas-Molist), Royal Society RG110591 (to V. Sanz-Moreno), and Barts Charity (to V. Sanz-Moreno and E. Crosas-Molist). E. Crosas-Molist was funded by Fundación Ramón Areces. I. Rodriguez-Hernandez was funded by Fundacion Alfonso Martin Escudero and Marie Sklodowska-Curie Action (H2020-MSCA-IF-2014-EF-ST).

The costs of publication of this article were defrayed in part by the payment of page charges. This article must therefore be hereby marked *advertisement* in accordance with 18 U.S.C. Section 1734 solely to indicate this fact.

Received April 17, 2019; revised August 27, 2019; accepted October 4, 2019; published first October 8, 2019.

References

1. Hanahan D, Weinberg RA. The hallmarks of cancer. Cell 2000;100:57–70.
2. Hanahan D, Weinberg RA. Hallmarks of cancer: the next generation. Cell 2011;144:646–74.
3. Turajlic S, Sottoriva A, Graham T, Swanton C. Resolving genetic heterogeneity in cancer. Nat Rev Genet 2019;20:404–16.
4. Martin-Martin N, Carracedo A, Torrano V. Metabolism and transcription in cancer: merging two classic tales. Front Cell Dev Biol 2017;5:119.
5. Spiegelman BM, Heinrich R. Biological control through regulated transcriptional coactivators. Cell 2004;119:157–67.
6. Finck BN, Kelly DP. PGC-1 coactivators: inducible regulators of energy metabolism in health and disease. J Clin Invest 2006;116:615–22.
7. Valcarcel-Jimenez L, Gaude E, Torrano V, Frezza C, Carracedo A. Mitochondrial metabolism: Yin and Yang for tumor progression. Trends Endocrinol Metab 2017;28:748–57.
8. Lin J, Handschin C, Spiegelman BM. Metabolic control through the PGC-1 family of transcription coactivators. Cell Metab 2005;1:361–70.
9. Carracedo A, Weiss D, Leliaert AK, Bhasin M, de Boer VC, Laurent G, et al. A metabolic prosurvival role for PML in breast cancer. J Clin Invest 2012;122:3088–100.
10. Haq R, Shoag J, Andreu-Perez P, Yokoyama S, Edelman H, Rowe GC, et al. Oncogenic BRAF regulates oxidative metabolism via PGC1alpha and MITF. Cancer Cell 2013;23:302–15.
11. Vazquez F, Lim JH, Chim H, Bhalla K, Girnun G, Pierce K, et al. PGC1alpha expression defines a subset of human melanoma tumors with increased mitochondrial capacity and resistance to oxidative stress. Cancer Cell 2013;23:287–301.
12. LeBleu VS, O'Connell JT, Gonzalez Herrera KN, Wikman H, Pantel K, Haigis MC, et al. PGC-1alpha mediates mitochondrial biogenesis and oxidative phosphorylation in cancer cells to promote metastasis. Nat Cell Biol 2014;16:992–1003.
13. Sancho P, Burgos-Ramos E, Tavera A, Bou Kheir T, Jagust P, Schoenhals M, et al. MYC/PGC-1alpha balance determines the metabolic phenotype and plasticity of pancreatic cancer stem cells. Cell Metab 2015;22:590–605.
14. Andrzejewski S, Klimcakova E, Johnson RM, Tabaries S, Annis MG, McGuirk S, et al. PGC-1alpha promotes breast cancer metastasis and confers bioenergetic flexibility against metabolic drugs. Cell Metab 2017;26:778–87.
15. LaGory EL, Wu C, Taniguchi CM, Ding CC, Chi JT, von Eyben R, et al. Suppression of PGC-1alpha is critical for reprogramming oxidative metabolism in renal cell carcinoma. Cell Rep 2015;12:116–27.
16. Luo C, Lim JH, Lee Y, Granter SR, Thomas A, Vazquez F, et al. A PGC1alpha-mediated transcriptional axis suppresses melanoma metastasis. Nature 2016;537:422–6.
17. Torrano V, Valcarcel-Jimenez L, Cortazar AR, Liu X, Urosevic J, Castillo-Martin M, et al. The metabolic co-regulator PGC1alpha suppresses prostate cancer metastasis. Nat Cell Biol 2016;18:645–56.
18. Kaminski L, Torrino S, Dufies M, Djabari Z, Haider R, Roustan FR, et al. PGC1alpha inhibits polyamine synthesis to suppress prostate cancer aggressiveness. Cancer Res 2019;79:3268–80.
19. Pandya P, Orgaz JL, Sanz-Moreno V. Modes of invasion during tumour dissemination. Mol Oncol 2017;11:5–27.
20. Wiederschain D, Wee S, Chen L, Loo A, Yang G, Huang A, et al. Single-vector inducible lentiviral RNAi system for oncology target validation. Cell Cycle 2009;8:498–504.
21. Carracedo A, Ma L, Teruya-Feldstein J, Rojo F, Salmena L, Alimonti A, et al. Inhibition of mTORC1 leads to MAPK pathway activation through a PI3K-dependent feedback loop in human cancer. J Clin Invest 2008;118:3065–74.
22. Georgouli M, Herraiz C, Crosas-Molist E, Fanshawe B, Maiques O, Perdrix A, et al. Regional activation of Myosin II in cancer cells drives tumor progression via a secretory cross-talk with the immune microenvironment. Cell 2019;176:757–74.
23. Crosas-Molist E, Bertran E, Rodriguez-Hernandez I, Herraiz C, Cantelli G, Fabra A, et al. The NADPH oxidase NOX4 represses epithelial to amoeboid transition and efficient tumour dissemination. Oncogene 2017;36:3002–14.
24. Ugalde-Olano A, Egia A, Fernandez-Ruiz S, Loizaga-Iriarte A, Zuniga-Garcia P, Garcia S, et al. Methodological aspects of the molecular and histological study of prostate cancer: focus on PTEN. Methods 2015;77–78:25–30.

25. Cortazar AR, Torrano V, Martín-Martín N, Caro-Maldonado A, Camacho L, Hermanova I, et al. CANCERTOOL: a visualization and representation interface to exploit cancer datasets. Cancer Res 2018;78:6320–8.
26. Jeannot P, Nowosad A, Perchey RT, Callot C, Bennana E, Katsube T, et al. p27(Kip1) promotes invadopodia turnover and invasion through the regulation of the PAK1/Cortactin pathway. Elife 2017; 6:pii:e22207.
27. Nadeem L, Brkic J, Chen YF, Bui T, Munir S, Peng C. Cytoplasmic mislocalization of p27 and CDK2 mediates the anti-migratory and anti-proliferative effects of Nodal in human trophoblast cells. J Cell Sci 2013;126:445–53.
28. Steller EJ, Borel Rinkes IH, Kranenburg O. How CD95 stimulates invasion. Cell Cycle 2011;10:3857–62.
29. Yoon H, Kim M, Jang K, Shin M, Besser A, Xiao X, et al. p27 transcriptionally coregulates cJun to drive programs of tumor progression. Proc Natl Acad Sci U S A 2019;116:7005–14.
30. Pandya P, Orgaz JL, Sanz-Moreno V. Actomyosin contractility and collective migration: may the force be with you. Curr Opin Cell Biol 2017;48: 87–96.
31. Bravo-Cordero JJ, Magalhaes MA, Eddy RJ, Hodgson L, Condeelis J. Functions of cofilin in cell locomotion and invasion. Nat Rev Mol Cell Biol 2013;14:405–15.
32. Hood JD, Cheresh DA. Role of integrins in cell invasion and migration. Nat Rev Cancer 2002;2:91–100.
33. Liu R, Zhang T, Zhu G, Xing M. Regulation of mutant TERT by BRAF V600E/MAP kinase pathway through FOS/GABP in human cancer. Nat Commun 2018;9:579.
34. Nakano T, Kanai Y, Amano Y, Yoshimoto T, Matsubara D, Shibano T, et al. Establishment of highly metastatic KRAS mutant lung cancer cell sublines in long-term three-dimensional low attachment cultures. PLoS One 2017; 12:e0181342.
35. Grasso CS, Wu YM, Robinson DR, Cao X, Dhanasekaran SM, Khan AP, et al. The mutational landscape of lethal castration-resistant prostate cancer. Nature 2012;487:239–43.
36. Lapointe J, Li C, Higgins JP, van de Rijn M, Bair E, Montgomery K, et al. Gene expression profiling identifies clinically relevant subtypes of prostate cancer. Proc Natl Acad Sci U S A 2004;101:811–6.
37. Taylor BS, Schultz N, Hieronymus H, Gopalan A, Xiao Y, Carver BS, et al. Integrative genomic profiling of human prostate cancer. Cancer Cell 2010; 18:11–22.
38. Wang P, Guo X, Zong W, Li Y, Liu G, Lv Y, et al. PGC-1alpha/SNAI1 axis regulates tumor growth and metastasis by targeting miR-128b in gastric cancer. J Cell Physiol 2019;234:17232–41.
39. Dan L, Wang C, Ma P, Yu Q, Gu M, Dong L, et al. PGC1alpha promotes cholangiocarcinoma metastasis by upregulating PDHA1 and MPC1 expression to reverse the Warburg effect. Cell Death Dis 2018;9: 466.
40. Gelato KA, Schockel L, Klingbeil O, Ruckert T, Lesche R, Toedling J, et al. Super-enhancers define a proliferative PGC-1alpha-expressing melanoma subgroup sensitive to BET inhibition. Oncogene 2018;37: 512–21.
41. Cruz-Bermudez A, Laza-Briviesca R, Vicente-Blanco RJ, Garcia-Grande A, Coronado MJ, Laine-Menendez S, et al. Cisplatin resistance involves a metabolic reprogramming through ROS and PGC-1alpha in NSCLC which can be overcome by OXPHOS inhibition. Free Radic Biol Med 2019;135: 167–81.
42. Gentric G, Kieffer Y, Mieulet V, Goundiam O, Bonneau C, Nemati F, et al. PML-regulated mitochondrial metabolism enhances chemosensitivity in human ovarian cancers. Cell Metab 2019;29:156–73.
43. Zhu J, Thompson CB. Metabolic regulation of cell growth and proliferation. Nat Rev Mol Cell Biol 2019;20:436–50.
44. Steeg PS. Targeting metastasis. Nat Rev Cancer 2016;16:201–18.
45. Jeon SM, Chandel NS, Hay N. AMPK regulates NADPH homeostasis to promote tumour cell survival during energy stress. Nature 2012;485: 661–5.
46. Carracedo A, Cantley LC, Pandolfi PP. Cancer metabolism: fatty acid oxidation in the limelight. Nat Rev Cancer 2013;13:227–32.
47. Stein RA, McDonnell DP. Estrogen-related receptor alpha as a therapeutic target in cancer. Endocr Relat Cancer 2006;13Suppl 1: S25–32.
48. Audet-Walsh E, Papadopoli DJ, Gravel SP, Yee T, Bridon G, Caron M, et al. The PGC-1alpha/ERRalpha axis represses one-carbon metabolism and promotes sensitivity to anti-folate therapy in breast cancer. Cell Rep 2016;14:920–31.